THE TRANSITION AND AUTOCORRELATION STRUCTURE OF TES PROCESSES

Part II: Special Cases

DAVID L. JAGERMAN
BENJAMIN MELAMED

NEC USA, Inc.
C&C Research Laboratories
4 Independence Way
Princeton, New Jersey 08540

To the Memory of Micha Yadin

ABSTRACT

TES (Transform-Expand-Sample) is a versatile class of stochastic sequences which can capture arbitrary marginals and a wide variety of sample path behavior and autocorrelation functions. In TES, the initial variate is uniform on [0,1) and the next variate is obtained recursively by taking the fractional part (i.e., modulo-1 reduction) of a linear autoregressive scheme. The uniform TES variates can then be further transformed to have arbitrary marginals. A companion paper (Part I) presented the general theory of TES processes. This paper (Part II) contains various examples which demonstrate the efficacy of the TES paradigm by comparing numerical and simulation-based calculations for a variety of TES autocorrelation functions. The results have applications to the modeling of autocorrelated sequences, particularly in a Monte Carlo simulation context.

Keywords and Phrases: autocorrelated variates, correlated variates, autocorrelation function, autocovariance function, Markov processes, autoregressive processes, Monte Carlo simulation, TES Processes and Methods

1 INTRODUCTION

TES (*Transform-Expand-Sample*) is a versatile class of stochastic sequences which can capture arbitrary marginals and a wide variety of sample path behavior and autocorrelation functions. A companion paper, Jagerman and Melamed (1992), presented the general theory of TES processes in some detail; this companion paper will henceforth be referred to as Part I for short. The present paper (henceforth to be referred to as Part II) is a sequel to Part I. It specializes the general theory of Part I to a variety of useful examples which demonstrate the efficacy of the TES paradigm, by comparing numerical and simulation-based calculations of TES autocorrelations. Specifically, we derive here explicit formulas for the quantities $\tilde{f}_V(i2\pi\nu)$, $|\tilde{D}_\xi(i2\pi\nu)|^2$ and $\tilde{D}^2_\xi(i2\pi\nu)$ whose real parts are used in Theorems 1-5 of Part I to compute transition densities of TES processes and autocorrelation functions of TES processes and their distorted (transformed) variants. The formulas derived here can then be used in numerical algorithms to implement the TES paradigm on a digital computer. A software implementation of a visual TES modeling environment, called TEStool, is described in Geist and Melamed (1991) and (1992), and briefly discussed in Section 6 of Part I.

Because the two parts are tightly coupled, we shall not summarize the TES theory already presented in Part I. Rather, we assume with few exceptions, that the reader has already consulted Part I as prerequisite material to Part II.

The rest of this paper is organized as follows. Section 2 treats a number of specialized innovations with special emphasis on mixtures of uniform innovations. Section 3 deals with a variety of continuous and discrete distortions; piecewise linear distortions are stressed, as such distortions applied to Uniform$(0,1)$ variates can approximate any empirical histogram arbitrarily closely. Section 4 gives closed form representation for the autocorrelation function of undistorted basic TES processes (those with uniform innovations and no stitching). Finally, Section 5 compares TES autocorrelation functions to their simulation-based counterparts. The comparison shows the numerical computation to be by far the faster and more accurate of the two, thereby enabling the heuristic computer-based approach to TES modeling reported in Geist and Melamed (1991) and (1992), and Section 6 of Part I.

2 SPECIALIZED INNOVATIONS

In this section we specialize the marginal densities f_V of the TES innovation process $\{V_n\}$. Our goal is to derive the Laplace Transform quantities $\tilde{f}_V(i2\pi\nu)$ required to evaluate the transition densities in Theorems 1 and 2 of Part I, and the autocorrelation functions in Theorems 3 and 4 of Part I. Practical considerations will steer us to the class of step function densities corresponding to uniform and mixtures of uniform innovations. However, we shall also demonstrate the difficulty inherent in using non-uniform innovations.

2.1 Uniform Innovations

Elementary innovations with Uniform(L, R) distribution have a density of the form

$$f_V(x) \ = \ \frac{1}{R-L}\, 1_{[L,R)}(x), \tag{2.1}$$

where $-0.5 < L < R < 0.5$. This case was studied in some detail in Section 3 of Part I; here we reproduce the Laplace Transform formulas for completeness. Recall that the parameterization (L, R) is equivalent to the parameterization (α, ϕ), where $\alpha \ = \ R-L$ and $\phi \ = \ \frac{R+L}{R-L}$.

Proposition 1 *For the innovation density (2.1),*

$$\tilde{f}_V(i2\pi\nu) \ = \ \frac{e^{-i\pi\nu\alpha\phi}\,\sin(\pi\nu\alpha)}{\pi\nu\alpha} \tag{2.2}$$

$$Re[\tilde{f}_V^{\tau}(i2\pi\nu)] \ = \ \cos(\pi\nu\alpha\phi\tau)\left(\frac{\sin(\pi\nu\alpha)}{\pi\nu\alpha}\right)^{\tau} \tag{2.3}$$

Proof From Eq. (3.10) in Part I,

$$\tilde{f}_V(s) \ = \ \frac{e^{-sL} - e^{-sR}}{s\alpha} \ = \ \frac{e^{s\alpha(1-\phi)/2} - e^{-s\alpha(1+\phi)/2}}{s\alpha} \tag{2.4}$$

Setting $s = i2\pi\nu$ in Eq. (2.4) readily yields Eq. (2.2). Eq. (2.3) now follows by a straightforward calculation (see Corollary 1 in Part I). $\square$

2.2 Mixtures of Uniform Innovations

Mixtures of elementary innovations consist of Uniform(L_k, R_k) variates with mixing probabilities P_k, where $1 \leq k \leq K$ for some $K \geq 1$. Such mixtures have step function densities of the form

$$f_V(x) \;=\; \sum_{k=1}^{K} \frac{P_k}{R_k - L_k}\, 1_{[L_k,R_k)}(x). \tag{2.5}$$

In the sequel, we shall routinely interchange the pairs (L_k, R_k) with the equivalent pairs (α_k, ϕ_k), where $\alpha_k \;=\; R_k - L_k$ and $\phi_k \;=\; \frac{R_k + L_k}{R_k - L_k}$, analoguously to the previous subsection. The class of step function densities (2.5) enjoys two important properties: they can approximate general densities arbitrarily closely, and yet are easy to specify and manipulate computationally.

Proposition 2 *For the innovation density (2.5),*

$$\tilde{f}_V(i2\pi\nu) \;=\; \sum_{k=1}^{K} P_k \,\frac{e^{-i\pi\nu\alpha_k\phi_k}\,\sin(\pi\nu\alpha_k)}{\pi\nu\alpha_k} \tag{2.6}$$

Proof Eq. (2.4) readily generalizes from uniform to mixtures of uniforms as

$$\tilde{f}_V(s) \;=\; \sum_{k=1}^{K} P_k\,\frac{e^{-sL_k} - e^{-sR_k}}{s\alpha_k} \;=\; \sum_{k=1}^{K} P_k\,\frac{e^{s\alpha_k(1-\phi_k)/2} - e^{-s\alpha_k(1+\phi_k)/2}}{s\alpha_k} \tag{2.7}$$

Eq. (2.6) follows by setting $s = i2\pi\nu$ in Eq. (2.7). □

We note in passing that Eq. (2.3) does not generalize to mixtures of uniform densities.

2.3 Exponential Innovations

Exponential innovations have a density of the form

$$f_V(x) \;=\; \lambda e^{-\lambda x}, \tag{2.8}$$

where λ is the rate parameter. The exponential density is included here to illustrate the penalty (in the form of increased complexity – conceptual and often computational) which typically results from choices of innovation densities outside the class of step functions (2.5).

Proposition 3 *For the innovation density (2.8),*

$$\tilde{f}_V(i2\pi\nu) \;=\; \lambda\, e^{-\ln(\sqrt{\lambda^2+4\pi^2\nu^2})}\, e^{-i\tan^{-1}(2\pi\nu/\lambda)} \tag{2.9}$$

$$Re[\tilde{f}_V^{\tau}(i2\pi\nu)] \;=\; \lambda^{\tau} e^{-\tau\ln(\sqrt{\lambda^2+4\pi^2\nu^2})} \cos(\tau\tan^{-1}(2\pi\nu/\lambda)) \tag{2.10}$$

Proof Taking logarithms of The Laplace Transform

$$\tilde{f}_V(s) \;=\; \frac{\lambda}{s+\lambda} \tag{2.11}$$

of (2.8) for $s = i2\pi\nu$ yields

$$\begin{aligned} \ln\left(\frac{\lambda}{\lambda + i2\pi\nu}\right) &= \ln(\lambda) - \ln(\lambda + i2\pi\nu) \\ &= \ln(\lambda) - \ln(\sqrt{\lambda^2+4\pi^2\nu^2}) - i\tan^{-1}(2\pi\nu/\lambda). \end{aligned}$$

Taking exponentials of both sides above yields (2.9), from which (2.10) readily follows. □

The complexity engendered by the familiar exponential density in proposition 3 suggests an alternative modeling approach. As mentioned before, a uniform approach would call for approximating a general density by step function densities to any degree of accuracy, though with increasing computational cost. Nevertheless, in view of the heuristic nature of the TES modeling methodology described in Part I, our experience has revealed no compelling need for using the full range of innovation densities beyond the class of step functions. Rather, the simplicity and ease of specifying and manipulating step function densities appear to far outweigh what minor refinements one might glean from more general innovation densities.

3 SPECIALIZED DISTORTIONS

In this section we specialize general distortions D and stitched distortions of the form $D_\xi(x) = D(S_\xi(x))$, where S_ξ is some stitching transformation; recall from Section 3 of Part I that S_1 is the identity, so $D_1 = D$. Our goal is to derive the Laplace Transform quantities $|\tilde{D}(i2\pi\nu)|^2$ and $Re[\tilde{D}(i2\pi\nu)^2]$ required to evaluate the autocorrelation functions in Theorems 3 and 4 of Part I. To this end we denote, $\tilde{D}(i2\pi\nu) = a_\nu + i\, b_\nu$ for $\nu = 1, 2, \ldots$, so that

$$|\tilde{D}(i2\pi\nu)|^2 = a_\nu^2 + b_\nu^2, \quad Re[\tilde{D}^2(i2\pi\nu)] = a_\nu^2 - b_\nu^2 \tag{3.1}$$

are entirely specified in terms of the real numbers a_ν and b_ν. For stitched distortions D_ξ, we use the analoguous notation $\tilde{D}_\xi(i2\pi\nu) = a_{\xi,\nu} + i\, b_{\xi,\nu}$. Theorem 5 in Part I relates $a_{\xi,\nu}$ and $b_{\xi,\nu}$ to $\tilde{D}$ via

$$\tilde{D}_\xi(i2\pi\nu) = \xi\, \tilde{D}(i2\pi\nu\xi) + (1-\xi)\, \tilde{D}(-i2\pi\nu(1-\xi)). \tag{3.2}$$

Note that (3.2) is consistent with (3.1), since for $\xi = 1$ we have $D_1 = D$, implying that $a_{\xi,\nu} = a_\nu$ and $b_{\xi,\nu} = b_\nu$.

The rest of the section derives the quantities $a_\nu,\ b_\nu,\ a_{\xi,\nu}$ and $b_{\xi,\nu}$ for a range of specialized distortions. Throughout this section, U always denotes a Uniform$(0, 1)$ variate and $X = D(U)$ denotes the corresponding distorted variate under a distortion $D(x),\ x \in [0, 1)$.

3.1 Piecewise-Linear Distortion (Mixture of Uniform Marginals)

In this subsection, we let $X = D(U)$ be a mixture of $N \geq 1$ Uniform(l_n, r_n) variates ($l_n < r_n$) with mixing probabilities p_n (we assume for simplicity that $p_n > 0,\ 1 \leq n \leq N$). Further, let $\{C_n\}_{n=0}^N$ be the cumulative distribution of $\{p_n\}_{n=1}^N$, where $C_n = \sum_{j=1}^n p_j$; note that $C_0 = 0$ and $C_N = 1$. Finally, denote $w_n = r_n - l_n$. Then X has the step function density

$$f_X(x) = \sum_{n=1}^N 1_{[l_n, r_n)}(x)\, \frac{p_n}{w_n} \tag{3.3}$$

and $D(x)$ is the piecewise-linear function

$$D(x) = \sum_{n=1}^N 1_{[C_{n-1}, C_n)}(x) \left[l_n + (x - C_{n-1})\, \frac{w_n}{p_n} \right]. \tag{3.4}$$

As in Subsection 2.2, we draw attention to the simplicity of specifying densities of the form (3.3). We reemphasize the fact that step function densities can approximate any density arbitrarily closely, and in practice, they are widely used in the form of histograms to model empirical densities.

Proposition 4 *For the piecewise-linear distortion (3.4),*

$$a_\nu = \sum_{n=1}^{N} \left[\frac{r_n \sin(2\pi\nu C_n) - l_n \sin(2\pi\nu C_{n-1})}{2\pi\nu} + \frac{\cos(2\pi\nu C_n) - \cos(2\pi\nu C_{n-1})}{(2\pi\nu)^2} \times \frac{w_n}{p_n} \right] \tag{3.5}$$

$$b_\nu = \sum_{n=1}^{N} \left[\frac{r_n \cos(2\pi\nu C_n) - l_n \cos(2\pi\nu C_{n-1})}{2\pi\nu} - \frac{\sin(2\pi\nu C_n) - \sin(2\pi\nu C_{n-1})}{(2\pi\nu)^2} \times \frac{w_n}{p_n} \right] \tag{3.6}$$

and for $0 < \xi < 1$,

$$\begin{aligned} a_{\xi,\nu} &= \sum_{n=1}^{N} \frac{r_n \left[\sin(2\pi\nu\xi C_n) + \sin(2\pi\nu(1-\xi)C_n)\right]}{2\pi\nu} \\ &- \sum_{n=1}^{N} \frac{l_n \left[\sin(2\pi\nu\xi C_{n-1}) + \sin(2\pi\nu(1-\xi)C_{n-1})\right]}{2\pi\nu} \\ &+ \sum_{n=1}^{N} \frac{w_n}{p_n} \left[\frac{\cos(2\pi\nu\xi C_n) - \cos(2\pi\nu\xi C_{n-1})}{\xi\,(2\pi\nu)^2} + \frac{\cos(2\pi\nu(1-\xi)C_n) - \cos(2\pi\nu(1-\xi)C_{n-1})}{(1-\xi)(2\pi\nu)^2} \right] \end{aligned} \tag{3.7}$$

$$\begin{aligned} b_{\xi,\nu} &= \sum_{n=1}^{N} \frac{r_n \left[\cos(2\pi\nu\xi C_n) - \cos(2\pi\nu(1-\xi)C_n)\right]}{2\pi\nu} \\ &- \sum_{n=1}^{N} \frac{l_n \left[\cos(2\pi\nu\xi C_{n-1}) - \cos(2\pi\nu(1-\xi)C_{n-1}\right]}{2\pi\nu} \\ &- \sum_{n=1}^{N} \frac{w_n}{p_n} \left[\frac{\sin(2\pi\nu\xi C_n) - \sin(2\pi\nu\xi C_{n-1})}{\xi\,(2\pi\nu)^2} - \frac{\sin(2\pi\nu(1-\xi)C_n) - \sin(2\pi\nu(1-\xi)C_{n-1})}{(1-\xi)(2\pi\nu)^2} \right] \end{aligned} \tag{3.8}$$

Proof The Laplace Transform of the piecewise-linear distortion (3.4) is

$$\tilde{D}(s) = \int_0^1 e^{-sx} \sum_{n=1}^{N} 1_{[C_{n-1},C_n)}(x) \left[l_n + (x - C_{n-1}) \frac{w_n}{p_n} \right] dx.$$

Interchanging summation and integration and calculating the integrals result in

$$\begin{aligned}
\tilde{D}(s) &= \sum_{n=1}^{N} \int_{C_{n-1}}^{C_n} e^{-sx} \left[l_n + (x - C_{n-1}) \frac{w_n}{p_n} \right] dx \\
&= \sum_{n=1}^{N} \left[\frac{e^{-sC_{n-1}} - e^{-sC_n}}{s} \left(l_n - C_{n-1} \frac{w_n}{p_n} \right) \right. \\
&\qquad \left. + \left(\frac{e^{-sC_{n-1}} - e^{-sC_n}}{s^2} + \frac{C_{n-1}\, e^{-sC_{n-1}} - C_n\, e^{-sC_n}}{s} \right) \frac{w_n}{p_n} \right] \\
&= \sum_{n=1}^{N} \left[\frac{l_n\, e^{-sC_{n-1}} - r_n\, e^{-sC_n}}{s} + \frac{e^{-sC_{n-1}} - e^{-sC_n}}{s^2} \times \frac{w_n}{p_n} \right] \qquad (3.9)
\end{aligned}$$

Setting $s = i2\pi\nu$ in (3.9) yields Eqs. (3.5) and (3.6) after writing the trigonometric representation of complex exponentials and collecting terms, through some moderately tedious algebra. For $0 < \xi < 1$, we calculate from (3.9) the quantities $\tilde{D}_\xi(i2\pi\nu)$ with the aid of (3.2); a similar, though more tedious, algebra finally yields Eqs. (3.7) and (3.8). □

For $N = 1$ we have $l_1 = l,\ r_1 = r$ and $C_1 = 1$; the distortion D then becomes

$$D(x) \;=\; l + (r - l)\, x \qquad (3.10)$$

which corresponds to the Uniform(l, r) marginal density

$$f_X(x) \;=\; \frac{1}{r - l}\, 1_{[l,r)}(x). \qquad (3.11)$$

We then obtain the following simplification

Proposition 5 *For the linear distortion (3.10),*

$$a_\nu \;=\; 0, \;\; b_\nu \;=\; \frac{r - l}{2\pi\nu} \qquad (3.12)$$

and for $0 < \xi < 1$,

$$a_{\xi,\nu} \;=\; \frac{r - l}{\xi(1-\xi)(2\pi\nu)^2}\, [\cos(2\pi\nu\xi) - 1], \;\; b_{\xi,\nu} \;=\; \frac{-(r - l)\, \sin(2\pi\nu\xi)}{\xi(1-\xi)(2\pi\nu)^2} \qquad (3.13)$$

Proof Just substitute the case $N = 1$ into Proposition 4 and simplify. □

We conclude by observing that The identity distortion $D(x) = x$ corresponds to $l = 0$ and $r = 1$, i.e., to an undistorted TES process with Uniform$(0, 1)$ marginals.

3.2 Step Function Distortion (Discrete Marginal)

In this subsection, we let $X = D(U)$ be a discrete variate with a countable state space J (finite or infinite) of integers. Further, let $\{v_j\}_{j \in J}$ be a real sequence, and let $\{p_j\}_{j \in J}$ be a discrete density function (i.e., $p_j > 0$ for all $j \in J$, and $\sum_{j \in J} p_j = 1$), with the interpretation that X assumes value v_j with probability p_j. Finally, let $\{C_j\}$ be the cumulative distribution function of $\{p_j\}$, where $C_j = \sum_{i=1}^{j} p_i$ (if J has a minimal element j_0, then we define $C_j = 0$ for $j < j_0$). Then X has the discrete density function

$$f_X(x) \;=\; \sum_{j \in J} 1_{\{v_j\}}(x)\, p_j, \tag{3.14}$$

and $D(x)$ is the step function

$$D(x) \;=\; \sum_{j \in J} 1_{[C_{j-1}, C_j)}(x)\, v_j. \tag{3.15}$$

Although discrete density functions can be obtained as limiting cases of step function densities, it is useful to treat them seperately (and exactly), as empirical histograms with a discrete component are likely to be encountered in practice.

Proposition 6 *For the step function distortion (3.15),*

$$a_\nu \;=\; \sum_{j \in J} v_j \, \frac{\sin(2\pi\nu C_j) - \sin(2\pi\nu C_{j-1})}{2\pi\nu} \tag{3.16}$$

$$b_\nu \;=\; \sum_{j \in J} v_j \, \frac{\cos(2\pi\nu C_j) - \cos(2\pi\nu C_{j-1})}{2\pi\nu} \tag{3.17}$$

and for $0 < \xi < 1$*,*

$$\begin{aligned} a_{\xi,\nu} \;=\; \sum_{j \in J} \frac{v_j}{2\pi\nu} \, [&\sin(2\pi\nu\xi C_j) \;-\; \sin(2\pi\nu\xi C_{j-1}) \\ &+\; \sin(2\pi\nu(1-\xi)C_j) \;-\; \sin(2\pi\nu(1-\xi)C_{j-1})] \end{aligned} \tag{3.18}$$

$$\begin{aligned} b_{\xi,\nu} \;=\; \sum_{j \in J} \frac{v_j}{2\pi\nu} \, [&\cos(2\pi\nu\xi C_j) \;-\; \cos(2\pi\nu\xi C_{j-1}) \\ &-\; \cos(2\pi\nu(1-\xi)C_j) \;+\; \cos(2\pi\nu(1-\xi)C_{j-1})] \end{aligned} \tag{3.19}$$

Proof The Laplace Transform of the step function distortion (3.15) is

$$\tilde{D}(s) \ = \ \int_0^1 e^{-sx} \sum_{j\in J} 1_{[C_{j-1},C_j)}(x)\, v_j\, dx.$$

An easy calculation yields

$$\tilde{D}(s) \ = \ \sum_{j\in J} \int_{C_{j-1}}^{C_j} e^{-sx}\, v_j\, dx \ = \ \sum_{j\in J} v_j \, \frac{e^{-sC_{j-1}} \ - \ e^{-sC_j}}{s}. \tag{3.20}$$

Thus, for (3.20), Eq. (3.2) becomes

$$\tilde{D}_\xi(i2\pi\nu) \ = \ \sum_{j\in J} \frac{v_j}{i2\pi\nu} \Big[e^{-i2\pi\nu\xi C_{j-1}} \ - \ e^{-i2\pi\nu\xi C_j} \\ - \ e^{i2\pi\nu(1-\xi)C_{j-1}} \ + \ e^{i2\pi\nu(1-\xi)C_j} \Big]. \tag{3.21}$$

For any $0 \le \xi \le 1$, Eqs. (3.18) and (3.19) can now be readily derived from Eq. (3.21) by writing the trigonometric representation of complex exponentials and identifying the real and imaginary parts. To obtain the special cases in Eqs. (3.16)-(3.17), it remains to set $\xi = 1$ in Eqs. (3.18) and (3.19), respectively. □

We now proceed to specialize Proposition 6 to a geometric marginal as an illustrative example of a discrete marginal distribution. Specifically, we select $J = \{0, 1, \ldots\}$, and for $j \in J$ we define $v_j = j$ and $p_j = (1-q)q^j$ for some $0 < q < 1$, so that $C_j = 1 - q^{j+1}$. Consequently, when $X = D(U)$ is geometric,

$$f_X(x) \ = \ \sum_{j=0}^{\infty} 1_j(x)\, (1-q)q^j \tag{3.22}$$

$$D(x) \ = \ \sum_{j=0}^{\infty} 1[x \in [1-q^j, 1-q^{j+1})]\, v_j. \tag{3.23}$$

Proposition 7 *For the distortion (3.23) corresponding to the geometric density (3.22),*

$$a_\nu \ = \ \sum_{j=1}^{\infty} \frac{1}{2\pi\nu} \sin(2\pi\nu q^j), \quad b_\nu \ = \ \sum_{j=1}^{\infty} \frac{1}{2\pi\nu} \left[1 - \cos(2\pi\nu q^j)\right] \tag{3.24}$$

and for $0 < \xi < 1$,

$$a_{\xi,\nu} \ = \ -\sum_{j=1}^{\infty} \frac{1}{2\pi\nu} \left[\sin(2\pi\nu\xi(1-q^j)) \ + \ \sin(2\pi\nu(1-\xi)(1-q^j))\right] \tag{3.25}$$

$$b_{\xi,\nu} \ = \ -\sum_{j=1}^{\infty} \frac{1}{2\pi\nu} \left[\cos(2\pi\nu\xi(1-q^j)) \ - \ \cos(2\pi\nu(1-\xi)(1-q^j))\right] \tag{3.26}$$

Proof Proposition 6 specializes to

$$a_{\xi,\nu} \;=\; \sum_{j=0}^{\infty} \frac{j}{2\pi\nu}\Big[\sin(2\pi\nu\xi(1-q^{j+1})) \;-\; \sin(2\pi\nu\xi(1-q^{j})) \\ +\; \sin(2\pi\nu(1-\xi)(1-q^{j+1})) \;-\; \sin(2\pi\nu(1-\xi)(1-q^{j}))\Big]$$

$$b_{\xi,\nu} \;=\; \sum_{j=0}^{\infty} \frac{j}{2\pi\nu}\Big[\cos(2\pi\nu\xi(1-q^{j+1}) \;-\; \cos(2\pi\nu\xi(1-q^{j})) \\ -\; \cos(2\pi\nu(1-\xi)(1-q^{j+1}) \;+\; \cos(2\pi\nu(1-\xi)(1-q^{j}))\Big]$$

These formulas can be further simplified with the aid of Abel's summation by parts formula (Bary (1964), p. 1), which states that for a real sequence $\{A_j\}$ satisfying $jA_j \longrightarrow 0$ as $j \uparrow \infty$, one has $\sum_{j=1}^{\infty} j(A_j - A_{j+1}) \;=\; \sum_{j=1}^{\infty} A_j$. To obtain Eq. (3.25), set in $a_{\xi,\nu}$ above

$$A_j \;=\; \frac{1}{2\pi\nu}\Big[-\sin(2\pi\nu\xi(1-q^{j})) - \sin(2\pi\nu(1-\xi)(1-q^{j}))\Big],$$

and to obtain Eq. (3.26), set in $b_{\xi,\nu}$ above

$$A_j \;=\; \frac{1}{2\pi\nu}\Big[-\cos(2\pi\nu\xi(1-q^{j})) + \cos(2\pi\nu(1-\xi)(1-q^{j}))\Big].$$

It is easily shown that the A_j in each case are $O(q^j)$ uniformly in ν and ξ; thus, the condition $jA_j \longrightarrow 0$ is met and the series (3.25) and (3.26) are uniformly convergent. Finally, to obtain Eq. (3.24), set $\xi = 1$ in Eqs. (3.25) and (3.26). □

3.3 Logarithmic Distortion (Exponential Marginal)

In this subsection, we let $X = D(U)$ be an Exponential(λ) variate with density function

$$f_X(x) \;=\; \lambda\, e^{-\lambda x}, \tag{3.27}$$

so D is the logarithmic distortion

$$D(x) \;=\; -\frac{\ln(1-x)}{\lambda}. \tag{3.28}$$

In the sequel, our calculations will heavily utilize the sine integral function

$$\mathcal{S}i(y) \;=\; \int_0^y \frac{\sin(x)}{x}\,dx \tag{3.29}$$

and the cosine integral function

$$\mathcal{C}i(y) \;=\; -\int_y^\infty \frac{\cos(x)}{x}\,dx \;=\; \gamma \,+\, \ln(y) \,-\, \int_0^y \frac{1-\cos(x)}{x}\,dx \tag{3.30}$$

where $\gamma \approx .57721566$ is Euler's constant. Numerical values for the sine and cosine integral functions are available, e.g., in Jahnke and Ende (1945). We shall also use the identities

$$\int_0^1 \cos(\theta x)\ln(x)\,dx \;=\; -\frac{1}{\theta}\int_0^1 \frac{\sin(\theta x)}{x}\,dx \;=\; -\frac{1}{\theta}\,\mathcal{S}i(\theta) \tag{3.31}$$

$$\int_0^1 \sin(\theta x)\ln(x)\,dx \;=\; -\frac{1}{\theta}\int_0^1 \frac{1-\cos(\theta x)}{x}\,dx \;=\; \frac{1}{\theta}\,[\mathcal{C}i(\theta)-\gamma-\ln(\theta)] \tag{3.32}$$

Finally, we shall simplify notation by using the two auxiliary functions

$$\mathcal{S}(\nu,\xi) \;=\; \mathcal{S}i(2\pi\nu\xi) \,+\, \mathcal{S}i(2\pi\nu(1-\xi)) \tag{3.33}$$

$$\mathcal{C}(\nu,\xi) \;=\; \mathcal{C}i(2\pi\nu\xi) \,-\, \mathcal{C}i(2\pi\nu(1-\xi)) \,+\, \ln((1-\xi)/\xi) \tag{3.34}$$

Proposition 8 *For the logarithmic distortion (3.28),*

$$a_\nu \;=\; \frac{\mathcal{S}i(2\pi\nu)}{2\pi\nu\lambda}, \quad b_\nu \;=\; -\frac{[\mathcal{C}i(2\pi\nu)-\gamma-\ln(2\pi\nu)]}{2\pi\nu\lambda} \tag{3.35}$$

and for $0<\xi<1$,

$$a_{\xi,\nu} \;=\; \frac{\cos(2\pi\nu\xi)}{2\pi\nu\lambda}\,\mathcal{S}(\nu,\xi) \,-\, \frac{\sin(2\pi\nu\xi)}{2\pi\nu\lambda}\,\mathcal{C}(\nu,\xi) \tag{3.36}$$

$$b_{\xi,\nu} \;=\; -\frac{\sin(2\pi\nu\xi)}{2\pi\nu\lambda}\,\mathcal{S}(\nu,\xi) \,-\, \frac{\cos(2\pi\nu\xi)}{2\pi\nu\lambda}\,\mathcal{C}(\nu,\xi) \tag{3.37}$$

Proof The Laplace Transform of (3.28) is

$$\tilde{D}(s) \;=\; -\frac{1}{\lambda}\int_0^1 e^{-sx}\ln(1-x)\,dx. \tag{3.38}$$

Setting $s=i2\pi\nu$ in (3.38) yields

$$\begin{aligned}\tilde{D}(i2\pi\nu) \;&=\; -\frac{1}{\lambda}\int_0^1 e^{-i2\pi\nu x}\,\ln(1-x)\,dx \;=\; -\frac{1}{\lambda}\int_0^1 e^{i2\pi\nu x}\,\ln(x)\,dx \\ &=\; -\frac{1}{\lambda}\int_0^1 \cos(2\pi\nu x)\,\ln(x)\,dx \,-\, \frac{i}{\lambda}\int_0^1 \sin(2\pi\nu x)\ln(x)\,dx.\end{aligned}$$

Eq. (3.35) now follows by substituting above the identities (3.31)-(3.32) for $\theta=2\pi\nu$.

Next, for $0 < \xi < 1$, we set the Laplace Transform (3.38) in Eq. (3.2) to obtain

$$
\begin{aligned}
\tilde{D}_\xi(i2\pi\nu) &= -\frac{\xi}{\lambda}\int_0^1 e^{-i2\pi\nu\xi x}\,\ln(1-x)\,dx \\
&\quad -\frac{1-\xi}{\lambda}\int_0^1 e^{i2\pi\nu(1-\xi)x}\ln(1-x)\,dx \\
&= -\frac{\xi}{\lambda}\int_0^1 e^{-i2\pi\nu\xi(1-x)}\ln(x)\,dx \\
&\quad -\frac{1-\xi}{\lambda}\int_0^1 e^{i2\pi\nu(1-\xi)(1-x)}\ln(x)\,dx.
\end{aligned}
$$

Taking real and imaginary parts above yields,

$$
\begin{aligned}
a_{\xi,\nu} &= -\frac{\xi}{\lambda}\int_0^1 \cos(2\pi\nu\xi(1-x))\ln(x)\,dx - \frac{1-\xi}{\lambda}\int_0^1 \cos(2\pi\nu(1-\xi)(1-x))\ln(x)\,dx \\
b_{\xi,\nu} &= \frac{\xi}{\lambda}\int_0^1 \sin(2\pi\nu\xi(1-x))\ln(x)\,dx - \frac{1-\xi}{\lambda}\int_0^1 \cos(2\pi\nu(1-\xi)(1-x))\ln(x)\,dx
\end{aligned}
$$

Using the formula for the cosine and sine functions of a difference, we get

$$
\begin{aligned}
a_{\xi,\nu} &= -\frac{\xi}{\lambda}\bigg[\cos(2\pi\nu\xi)\int_0^1 \cos(2\pi\nu\xi x)\ln(x)\,dx \\
&\qquad + \sin(2\pi\nu\xi)\int_0^1 \sin(2\pi\nu\xi x)\ln(x)\,dx\bigg] \\
&\quad -\frac{1-\xi}{\lambda}\bigg[\cos(2\pi\nu(1-\xi))\int_0^1 \cos(2\pi\nu(1-\xi)x)\ln(x)\,dx \\
&\qquad + \sin(2\pi\nu(1-\xi))\int_0^1 \sin(2\pi\nu(1-\xi)x)\ln(x)\,dx\bigg]
\end{aligned}
$$

and

$$
\begin{aligned}
b_{\xi,\nu} &= \frac{\xi}{\lambda}\bigg[\sin(2\pi\nu\xi)\int_0^1 \cos(2\pi\nu\xi x)\ln(x)\,dx \\
&\qquad - \cos(2\pi\nu\xi)\int_0^1 \sin(2\pi\nu\xi x)\ln(x)\,dx\bigg] \\
&\quad -\frac{1-\xi}{\lambda}\bigg[\sin(2\pi\nu(1-\xi))\int_0^1 \cos(2\pi\nu(1-\xi)x)\ln(x)\,dx \\
&\qquad - \cos(2\pi\nu(1-\xi))\int_0^1 \sin(2\pi\nu(1-\xi)x)\ln(x)\,dx\bigg]
\end{aligned}
$$

The rest follows from identities (3.31) and (3.32) for $\theta = 2\pi\nu\xi$ or $\theta = 2\pi\nu(1-\xi)$, and then collecting terms with the aid of Eqs. (3.33) and (3.34). □

4 UNIFORM INNOVATIONS AND IDENTITY DISTORTION

In this section, we let $\{U_n\}$ be an undistorted basic TES process, i.e., an unstitched TES(L, R) process (equivalently, TES(α, ϕ) process). Thus, throughout this section we employ uniform innovations $V_n \sim$ Uniform(L, R), the null stitching ($\xi = 1$), and the identity distortion (whence $X_n = U_n$). The case of undistorted basic TES processes was studied in some detail in Melamed (1991), mainly via Monte Carlo simulation. Such processes are basic in the sense that they span a relatively simple class of TES processes, yet this class exhibits a surprisingly versatile sample path behavior and a variety of autocorrelation function patterns.

Recall that uniform innovation densities have already been treated in Proposition 1; recall also that the identity distortion follows as a special case by setting $l = 0$ and $r = 1$ in Proposition 5. In this section, we improve on Proposition 5, by obtaining closed form formulas for the autocorrelations of undistorted basic TES processes with the aid of the auxiliary functions

$$\psi_c(\tau) \;=\; \frac{1}{\alpha^\tau} \sum_{k=0}^{\tau} \binom{\tau}{k} (-1)^k \sum_{\nu=1}^{\infty} \frac{2\,\cos(2\pi\nu(-L\tau - \alpha\nu))}{(2\pi\nu)^{\tau+2}}, \tag{4.1}$$

and

$$\psi_s(\tau) \;=\; \frac{1}{\alpha^\tau} \sum_{k=0}^{\tau} \binom{\tau}{k} (-1)^k \sum_{\nu=1}^{\infty} \frac{2\,\sin(2\pi\nu(-L\tau - \alpha\nu))}{(2\pi\nu)^{\tau+2}}. \tag{4.2}$$

We begin by deriving the autocovariance functions $\psi_U^+(\tau)$ and $\psi_U^-(\tau)$.

Proposition 9 *For an undistorted basic TES(L, R) process, and lags $\tau = 0, 1, \ldots$*

$$\psi_U^+(\tau) \;=\; \begin{cases} \psi_c(\tau), & \textit{if } \tau \equiv 0 \pmod 4 \\ \psi_s(\tau), & \textit{if } \tau \equiv 1 \pmod 4 \\ -\psi_c(\tau), & \textit{if } \tau \equiv 2 \pmod 4 \\ -\psi_s(\tau), & \textit{if } \tau \equiv 3 \pmod 4 \end{cases} \tag{4.3}$$

and

$$\psi_U^-(\tau) \;=\; \begin{cases} \psi_c(\tau), & \textit{if } \tau \equiv 0 \pmod 4 \\ -\psi_s(\tau), & \textit{if } \tau \equiv 1 \pmod 4 \\ -\psi_c(\tau), & \textit{if } \tau \equiv 2 \pmod 4 \\ \psi_s(\tau), & \textit{if } \tau \equiv 3 \pmod 4 \end{cases} \tag{4.4}$$

Proof It suffices to prove Eq. (4.3), since Eq. (4.4) easily follows from the relation $\psi_U^-(\tau) = (-1)^\tau \psi_U^+(\tau)$; see Part I, Eq. (3.6).

Now, from Theorem 3 in Part I, we deduce

$$\psi_U^+(\tau) = 2\sum_{\nu=1}^{\infty} Re\left[\left(\frac{e^{-i2\pi\nu L} - e^{-i2\pi\nu R}}{i2\pi\nu\alpha}\right)^\tau\right]\left(\frac{1}{2\pi\nu}\right)^2$$

where $Re[\tilde{f}_V^\tau(i2\pi\nu)$ was substituted from Eq. (2.4) in Proposition 1 for $s = i2\pi\nu$, whereas $a_\nu = 0$ and $b_\nu = \dfrac{1}{2\pi\nu}$ were obtained from Eq. (3.12) in Proposition 5, for $l = 0$ and $r = 1$. Applying the Binomial expansion to the powers of τ above yields

$$\begin{aligned}\psi_U^+(\tau) &= \sum_{\nu=1}^{\infty}\frac{2}{\alpha^\tau(2\pi\nu)^{\tau+2}} Re\left[i^{-\tau}\sum_{k=0}^{\tau}\binom{\tau}{k}(-1)^k e^{i2\pi\nu(-L\tau-\alpha k)}\right]\\ &= \alpha^{-\tau}\sum_{k=0}^{\tau}\binom{\tau}{k}(-1)^k\sum_{\nu=1}^{\infty}\frac{2}{(2\pi\nu)^{\tau+2}} Re\left[i^{-\tau}e^{i2\pi\nu(-L\tau-\alpha k)}\right].\end{aligned}$$

The result now follows by noting in succession that

$$i^{-\tau} = \begin{cases} 1, & if\ \tau \equiv 0 \pmod 4\\ -i, & if\ \tau \equiv 1 \pmod 4\\ -1, & if\ \tau \equiv 2 \pmod 4\\ i, & if\ \tau \equiv 3 \pmod 4\end{cases}$$

□

Formulas (4.3) and (4.4) reveal an interesting connection with Bernoulli polynomials. Extending the Bernoulli polynomials (denoted by $B_n(x)$) periodically (with period 1) from their restriction to the interval $[0, 1]$ to the real line yields the Bernoulli functions (denoted by $\bar{B}_n(x)$). It is known that the latter have the representation (Knopp (1946)),

$$\bar{B}_n(x) = \begin{cases} (-1)^{n/2+1}\, n!\displaystyle\sum_{\nu=1}^{\infty}\frac{2\cos(2\pi\nu x)}{(2\pi\nu)^n}, & n\ even\\ (-1)^{(n+1)/2}\, n!\displaystyle\sum_{\nu=1}^{\infty}\frac{2\sin(2\pi\nu x)}{(2\pi\nu)^n}, & n\ odd\end{cases} \tag{4.5}$$

A closed form representation for $\rho_U^+(\tau)$ and $\rho_U^-(\tau)$ can now be given in terms of the Bernoulli functions (4.5).

Proposition 10 *For an undistorted basic TES(L, R) process, and lags $\tau = 0, 1, \ldots$*

$$\rho_U^+(\tau) \;=\; \frac{12}{\alpha^\tau\,(\tau+2)!}\sum_{k=0}^{\tau}\binom{\tau}{k}(-1)^k\bar{B}_{\tau+2}(-L\tau-\alpha k) \tag{4.6}$$

$$\rho_U^-(\tau) \;=\; \frac{(-1)^\tau 12}{\alpha^\tau\,(\tau+2)!}\sum_{k=0}^{\tau}\binom{\tau}{k}(-1)^k\bar{B}_{\tau+2}(-L\tau-\alpha k) \tag{4.7}$$

Proof Immediate from Proposition 9 and Eq. (4.5), on dividing by $\sigma_U^2 = \frac{1}{12}$. $\square$

Note that Eqs. (4.6) and (4.7) confirm that $\rho_U^-(\tau) = (-1)^\tau\,\rho_U^+(\tau)$, in agreement with Eq. (3.6) in Part I. It is also instructive to obtain an explicit formula for the cases $\tau = 0$ and $\tau = 1$ from Eqs. (4.6) and (4.7). For $\tau = 0$, we see that $\rho_U^+(0) = \rho_U^-(0) = 1$; and for $\tau = 1$, we obtain a simple biquadratic expression in α and ϕ,

$$\rho_U^+(1) \;=\; 1 \;-\; \frac{3(1+\phi^2)}{2}\,\alpha \;+\; \frac{1+3\phi^2}{2}\,\alpha^2, \quad 0 \le \alpha, \phi \le 1 \tag{4.8}$$

in agreement with Theorem 1 in Melamed (1991).

5 DISCUSSION

Theorems 3-5 in Part I provide the theoretical basis for a numerical approach to the calculation of the autocorrelation functions of TES sequences and their distorted variants (refer to the concluding section of Part I). The specializations of Sections 2-3 in Part II give rise to fast and efficient algorithms amenable to computer implementation. These have been implemented in a visual modeling environment as reported in Geist and Melamed (1991) and (1992).

To check the efficacy of this approach as outlined in Part I and the numerical recipes presented in Part II, we compared the numerical algorithms against Monte Carlo simulations for a range of special cases. Each simulation run generated a TES sequence of 10^6 observations, from which the corresponding autocorrelation function was estimated by the standard statistics (see, e.g., Law and Kelton (1991), p. 285).

Figures 1-18 summarize the comparison. The figures are arranged in pairs where each odd-numbered member displays a sample path or a histogram obtained from a simulation run, and the adjacent even-numbered member displays the corresponding pair of TES autocorrelation functions: one calculated statistically from the simulation run (bullets), and the other computed numerically from the formulas presented in this paper (bars). An examination of the even-numbered autocorrelation figures supports the efficacy of the numerical algorithms. As evidenced by the graphs, the agreement is excellent (tabulated printouts displayed the same accuracy for a large variety of additional cases). We found that 100 terms were quite ample to achieve very good approximations, when truncating the infinite sums in Theorems 3 and 4 in Part I. Furthermore, while the statistical calculations from the simulation samples took on the order of minutes to complete, their numerical counterparts took well under one second (all runs were made on a SUN SPARCstation 2 workstation).

Figures 1-8 show four examples, depicting four fundamental behavioral modes of undistorted basic TES(α, ϕ) background sequences; recall from Section 3 of Part I, that the term 'basic' refers to unstitched TES processes with uniform innovations. An examination of the sample paths (Figures 1, 3, 5 and 7) reveals a qualitative difference between TES processes without drift ($\phi = 0$) in Figures 1 and 5, and those with drift ($\phi = 0.5$) in Figures 3 and 7. The latter exhibit a distinct cyclical structure resulting from periodic drifting across the "origin" on the unit circle. This cyclical structure is absent for $\phi = 0$, because the resulting random walk is not directional. Subsequently, the behavior of the corresponding autocorrelation functions (Figures 2, 4, 6 and 8) displays four functional forms. The driftless TES$^+$ case in Figure 2 is monotone decreasing, whereas the driftless TES$^-$ case in Figure 6 is alternating with monotone decreasing envelope. The TES$^+$ case with drift in Figure 4 is oscillatory, whereas its TES$^-$ counterpart in Figure 8 is simultaneously alternating and oscillatory. All autocorrelation functions are bounded by envelopes with monotone decreasing magnitude. The effect of increasing the magnitude of ϕ on sample path behavior is to decrease the mean "cycle time" of the directional random walk around the unit circle, with the corresponding autocorrelation function oscillating more rapidly. As expected, we found that an increase in α causes a decrease in the magnitude of the resultant autocorrelation functions for all lags.

The effect of stitching is demonstrated in Figures 9 and 10. Figure 9 is a stitched version ($\xi = 0.5$) of Figure 1. Notice how the "discontinuities" in the sample path of Figure 1 (the two spikes around serial numbers 400 and 420, and the dip around serial number 470) have been eliminated in Figure 9; the latter has an overall "continuous" appearance. We have found that stitching has the effect of increasing the magnitude of the autocorrelation function, as evidenced by Figures 10 and 2. The explanation for these TES$^+$ processes invokes the fact that crossings of the point 0 in either direction (from large values to small ones or vice versa) introduce a negative component into the autocorrelations of unstitched processes, and this negative component is eliminated in stitched ones.

Figures 11-16 demonstrate the effect of distortion on sample paths and autocorrelation functions of distorted basic TES sequences. A comparison of each distorted foreground sample path with its background counterpart reveals that certain visual features are preserved under unstitched distortions; this is due to the fact that unstitched distortions are monotonic, and each of those was applied to the same background sequence. For example, comparing various sample paths with exponential marginals (Figures 11 and 13) to the corresponding background TES sequences (respectively, Figures 1 and 5), we see that the general appearance of the sample path envelopes is quite similar, though the scales are different. In particular, the sample path "discontinuities" alluded to before are easily identifiable at the same serial numbers. The same observations hold when comparing the marginally geometric sample path in Figure 15 to its background counterpart in Figure 1, even though the the discrete-valued geometric case has a more "clipped" appearance than its continuous-valued counterparts. We mention that the visual "shadow" appearance of TES$^-$ sample paths (Figures 5, 7 and 13) is due to the alternation of large and small values, which gives rise to a negative lag-1 autocorrelation. An examination of the autocorrelation functions shows that the functional form is largely preserved under distortion, up to scaling. Thus, the autocorrelation functions in Figures 2, 12 and 16 are monotone decreasing, whereas those in Figures 6 and 14 are alternating. Our experience shows that the same effect holds for all other functional forms (oscillatory etc.) of TES autocorrelation functions. Note, however, that the scaling discrepancy between the exponential case (Figures 12) and the geometric case (Figure 16) is minimal. This should not be surprising since the two are (memoryless) analogues of each other. In fact, it can be shown (but we omit the proof) that the functions $\tilde{D}_E(i2\pi\nu)$ (for the exponential case) and $\tilde{D}_G(i2\pi\nu)$ (for the geometric case) are related by

$$\tilde{D}_G(i2\pi\nu) \approx \frac{\tilde{D}_E(i2\pi\nu)}{\ln(1/q)} + \frac{\pi\nu}{6}\ln(1/q) \quad \text{as} \;\; \text{q} \uparrow 1,$$

so they differ significantly only for small q (we have $q = 0.5$). On the other hand, Comparing Figure 14 to 6 suggests that distortion of TES$^-$ sequences gives rise to additional effects other than scaling. Specifically, note that the upper and lower envelopes bounding the autocorrelation function of the exponential case (Figure 14) are far less symmetric than their uniform counterparts (Figure 6). This observation accords with the well-known result (Ripley (1987), p. 129) that the extremal positive correlation coefficient of exponential variates can attain 1, whereas its extremal negative counterpart can only attain about -0.645, well short of -1.

We conclude our set of examples with a complicated example (see Figures 17 and 18), incorporating mixtures of uniform innovations, stitching and a histogram-based distortion. This example comprises a TES traffic model based on field mesurements of stochastic bitrate sequences (in this case a football scene) generated by compressed video frames in a high-speed communications network (see Lee et al. (1992) and Melamed et al. (1992)). From the empirical sample path we calculated the empirical histogram (Figure 17) and the empirical autocorrelation function (not shown). First, the distortion was defined as the inverse of the cumulative histogram corresponding to Figure 17; note the close match between the histograms of the simulated TES model and the empirical data. Next, A TES$^+$ model was deemed appropriate in view of the visual form of the empirical data. Finally, a heuristic search was conducted with TEStool (see Geist and Melamed (1991) and (1992) and Section 6 of Part I) for a stitching parameter and an innovation with a step function density, such that the autocorrelation function of the resultant stitched and distorted TES model approximated well the initial segment of its empirical counterpart (not shown). The search resulted in a background TES$^+$ model with $\xi = 0.5$ and a step function innovation density whose parameters are listed in the figures' headings. Figure 18 shows that the numerically computed autocorrelation function of the model agrees closely with the corresponding simulation statistics.

Additional insight into TES processes can be gained by investigating their spectral properties. This work is in progress and will be reported elsewhere.

References

[1] Bary, N. K. (1964) *A Treatise on Trigonometric Series*, MacMillan.

[2] Geist, D. and Melamed, B. (1991) "TEStool: A Visual Interactive Environment for Modeling Autocorrelated Time Series", *Preprint*, NEC USA, Inc., Princeton, NJ

[3] Geist, D. and Melamed, B. (1992) "TEStool: An Environment for Visual Interactive Modeling of Autocorrelated Traffic", *Proceedings of ICC '92*, Chicago, Illinois (to appear).

[4] Jagerman, D. L. and Melamed, B. (1992) "The Transition and Autocorrelation Structure of TES Processes Part I: General Theory", *Stochastic Models* (to appear).

[5] Jahnke, E. and Ende, F. (1945) *Tables of Functions with Formulae and Curves*, Dover Publications.

[6] Knopp, K. (1946) *Theory and Application of Infinite Series*, Blackie and Son, London and Glasgow.

[7] Law, A. M. and Kelton, D. W. (1991) *Simulation Modeling and Analysis*, 2nd edition, McGraw-Hill.

[8] Lee, D-S., Melamed, B., Reibman, A. R. and Sengupta, B. (1991) "Analysis of a Video Multiplexer Using TES as a Modeling Methodology", *Proceedings of GLOBCOM '91*, 1.3.1-1.3.5, Phoenix, Arizona.

[9] Melamed, B. (1991) "TES: A Class of Methods for Generating Autocorrelated Uniform Variates", *ORSA J. on Computing* 3(4), 317-329.

[10] Melamed, B., Raychaudhuri, D., Sengupta, B. and Zdepski, J. (1992) "TES-Based Traffic Modeling For Performance Evaluation of Integrated Networks", *Proceedings of INFOCOM '92*, Florence, Italy (to appear).

[11] Ripley, B. D. (1987) *Stochastic Simulation*, Wiley.

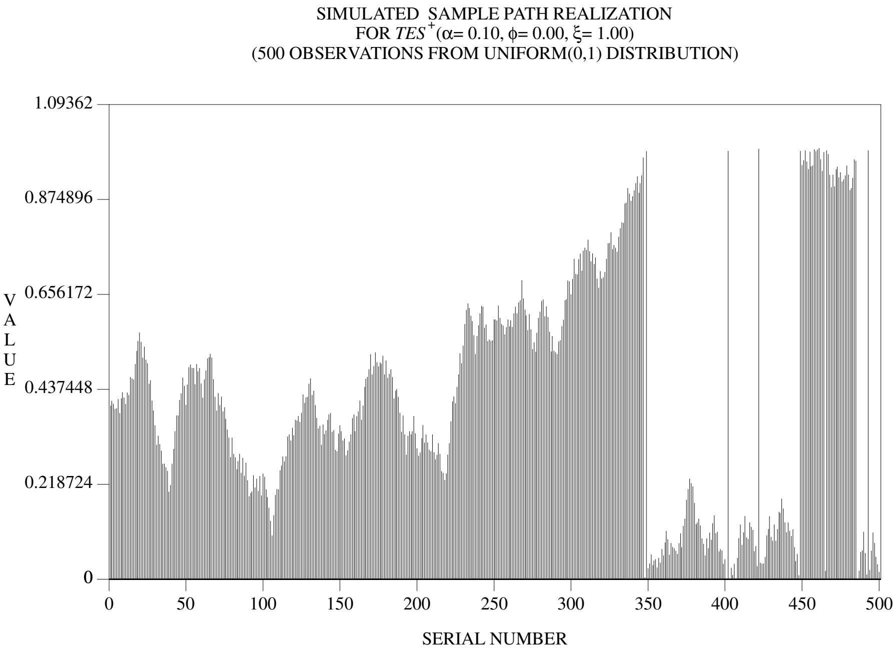

Figure 1: Sample Path of a Uniform TES$^+$ Process Without Drift

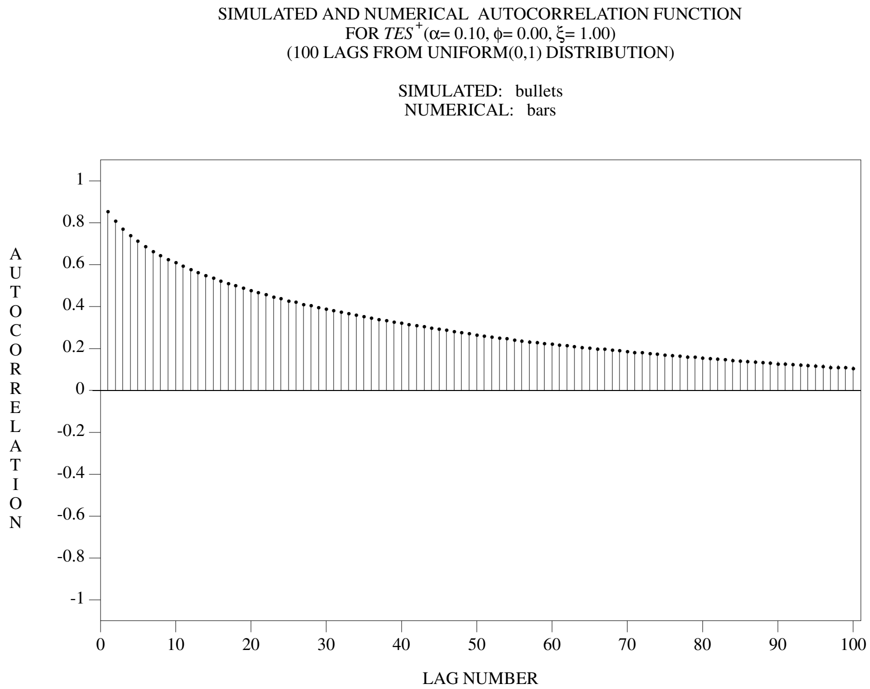

Figure 2: Autocorrelation Functions of a Uniform TES$^+$ Process Without Drift

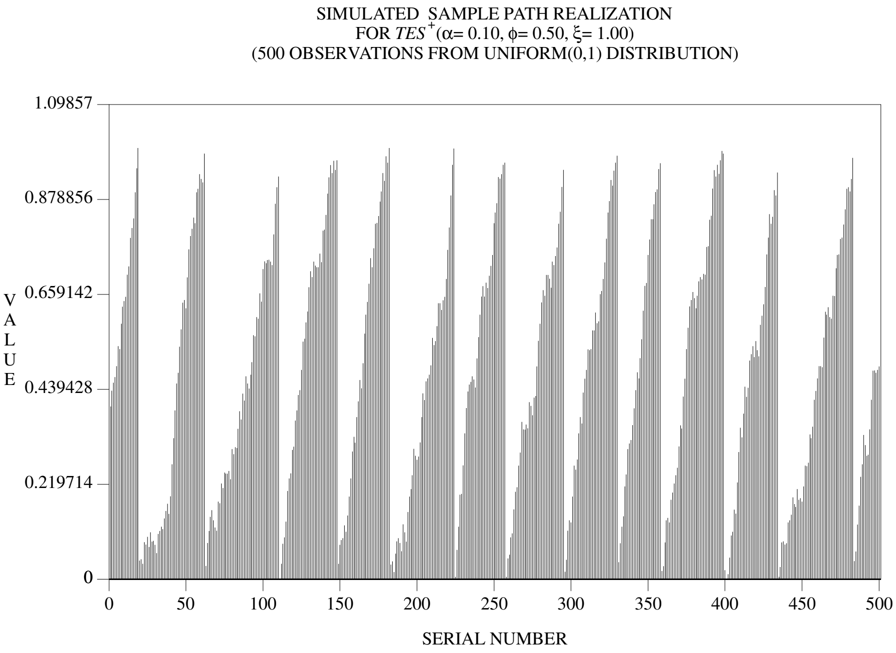

Figure 3: Sample Path of a Uniform TES$^+$ Process With Drift

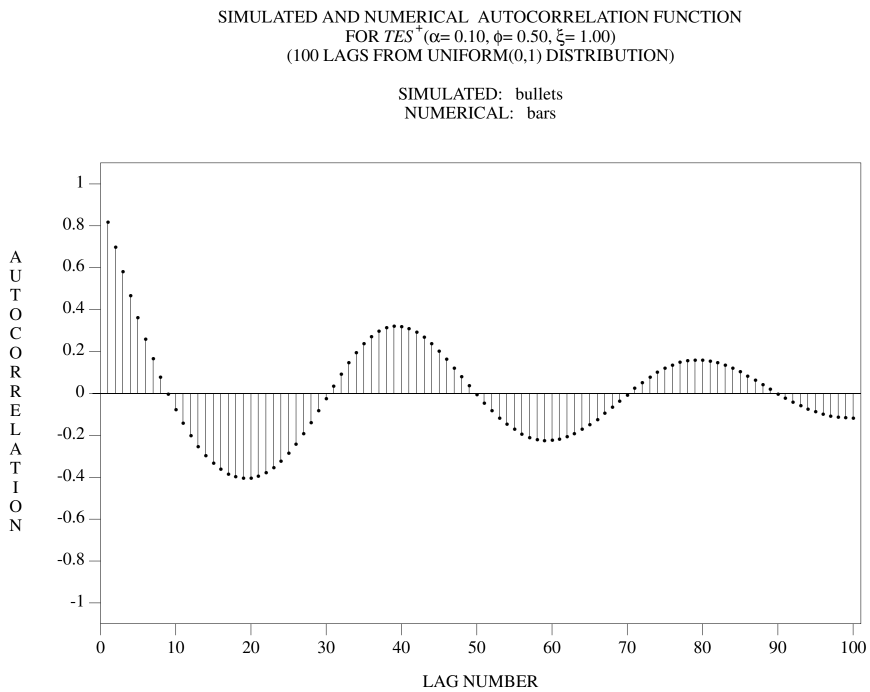

Figure 4: Autocorrelation Functions of a Uniform TES$^+$ Process With Drift

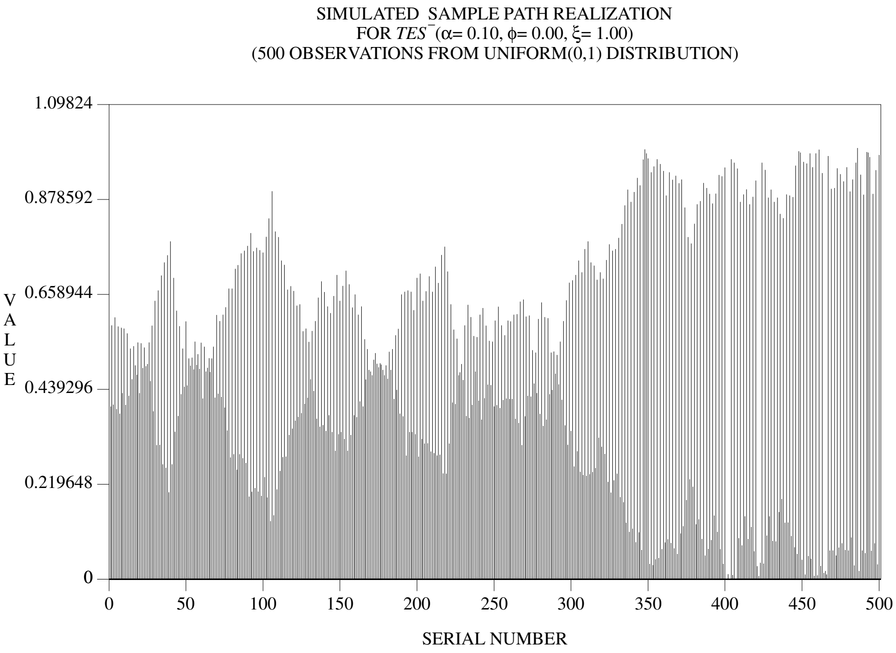

Figure 5: Sample Path of a Uniform TES^{-} Process Without Drift

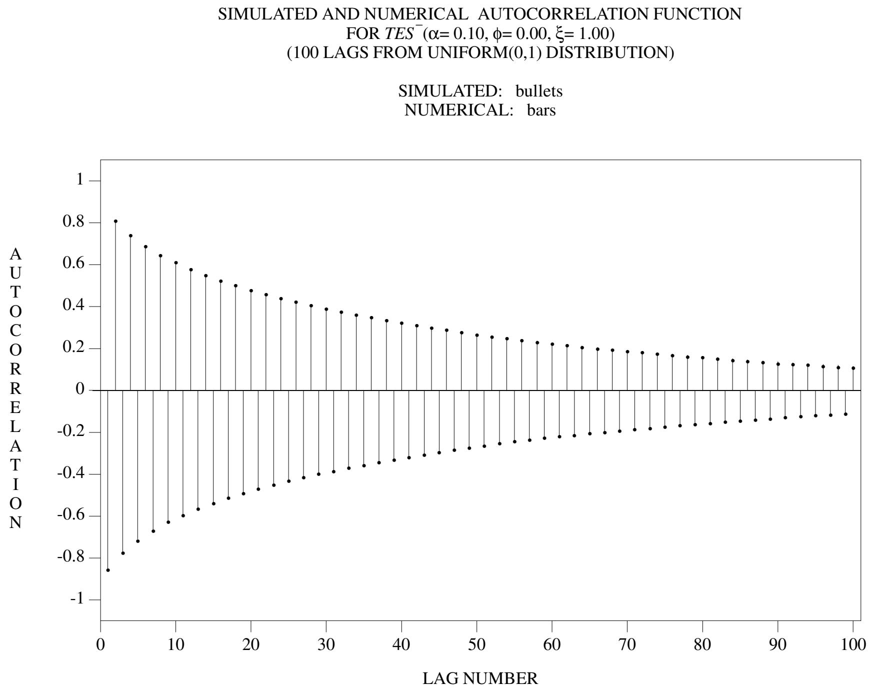

Figure 6: Autocorrelation Functions of a Uniform TES^{-} Process Without Drift

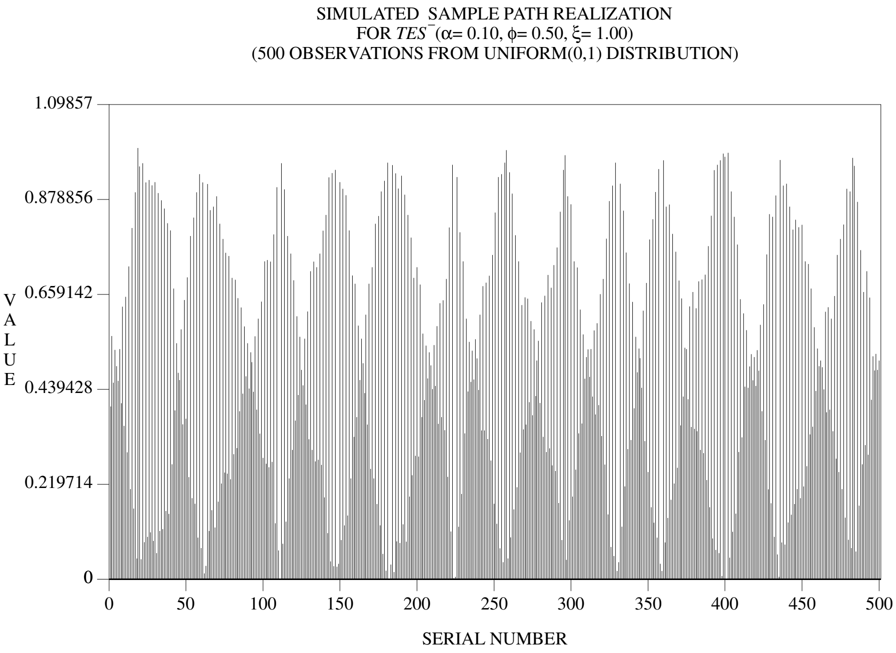

Figure 7: Sample Path of a Uniform TES$^-$ Process With Drift

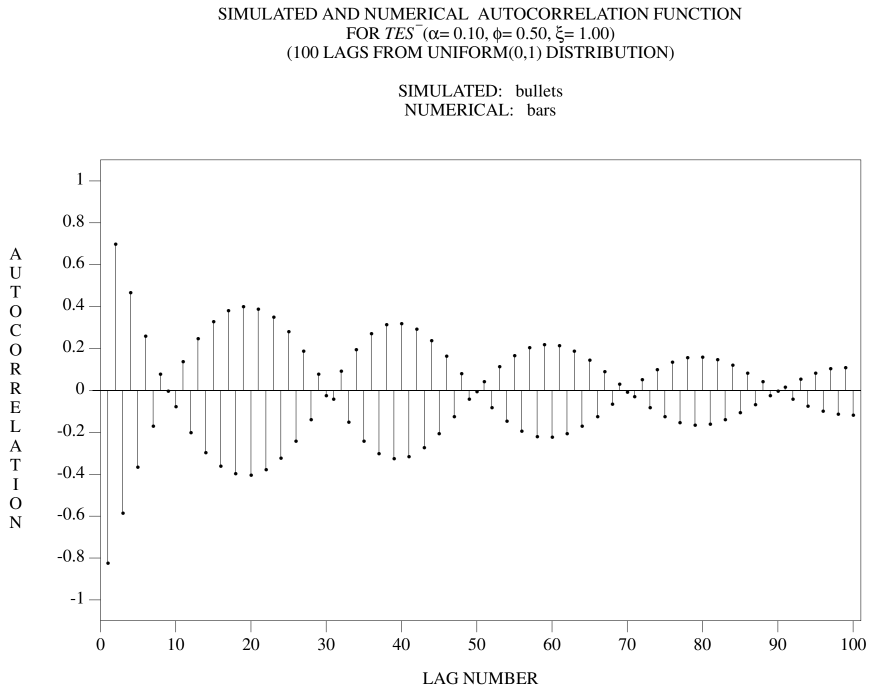

Figure 8: Autocorrelation Functions of a Uniform TES$^-$ Process With Drift

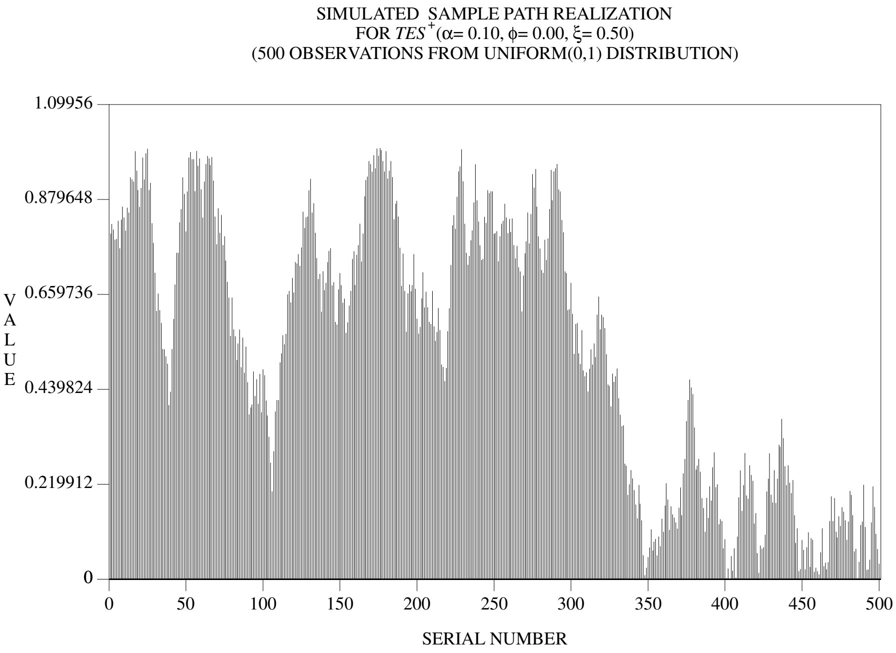

Figure 9: Sample Path of a Uniform Stitched Driftless TES$^+$ Process

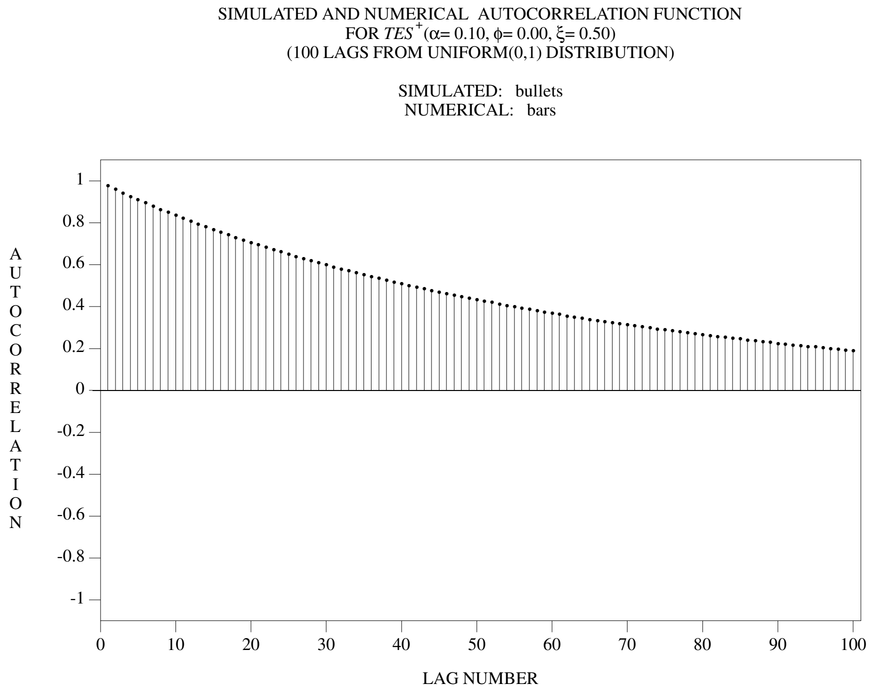

Figure 10: Autocorrelation Functions of a Uniform Stitched Driftless TES$^+$ Process

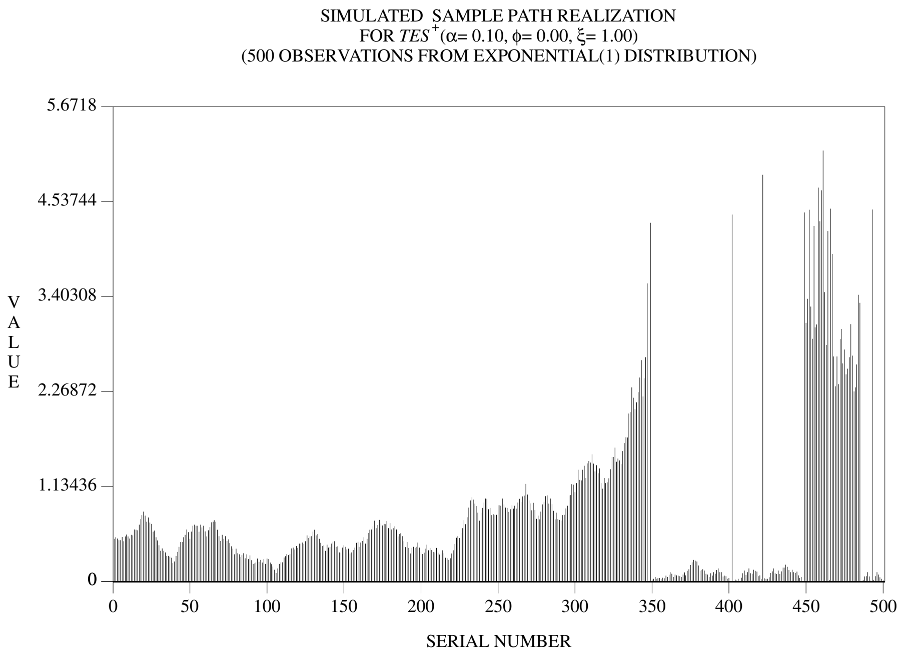

Figure 11: Sample Path of an Exponential TES$^+$ Process Without Drift

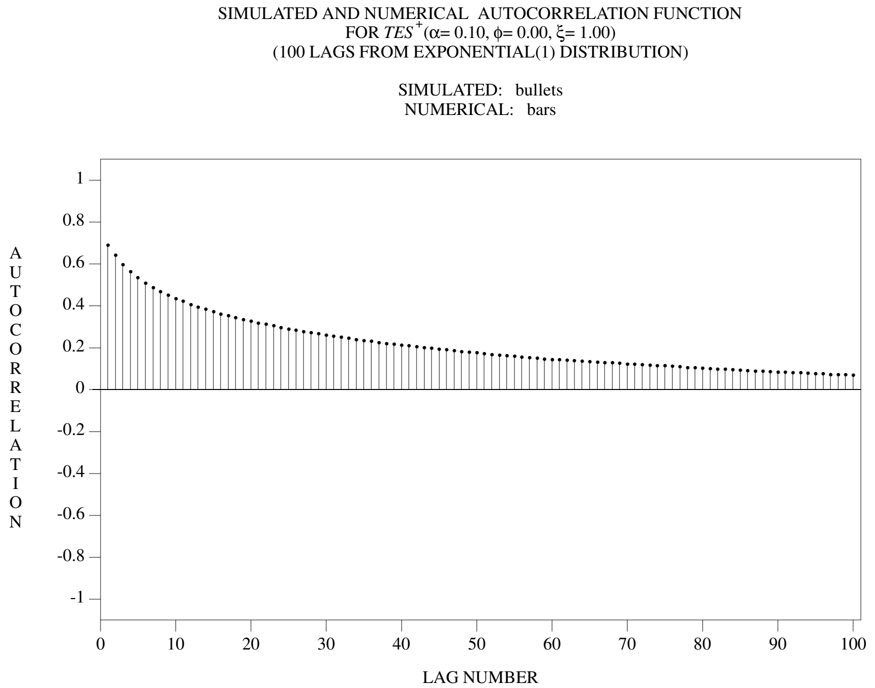

Figure 12: Autocorrelation Functions of an Exponential TES$^+$ Process Without Drift

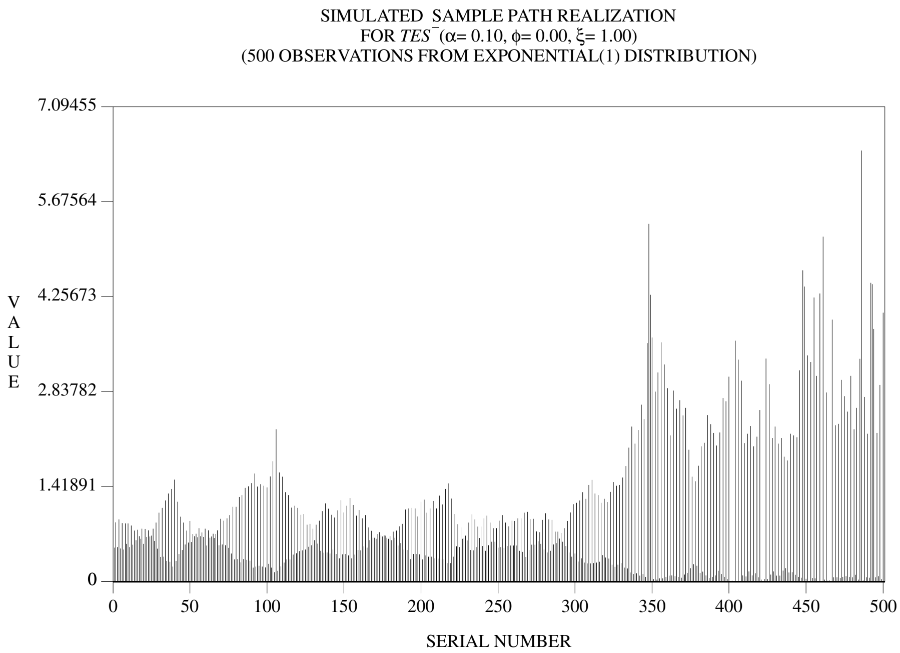

Figure 13: Sample Path of an Exponential TES$^-$ Process Without Drift

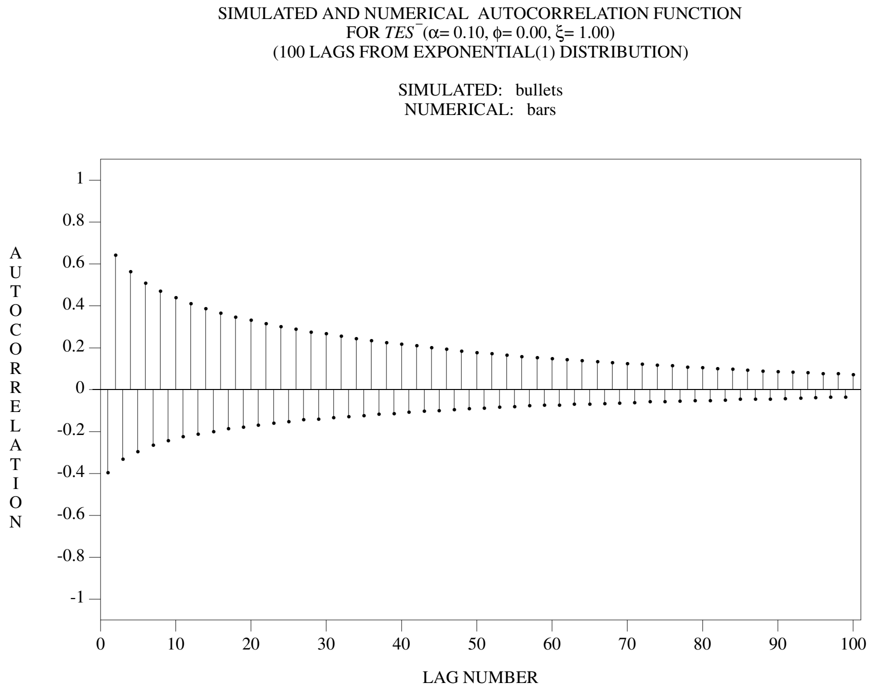

Figure 14: Autocorrelation Functions of an Exponential TES$^-$ Process Without Drift

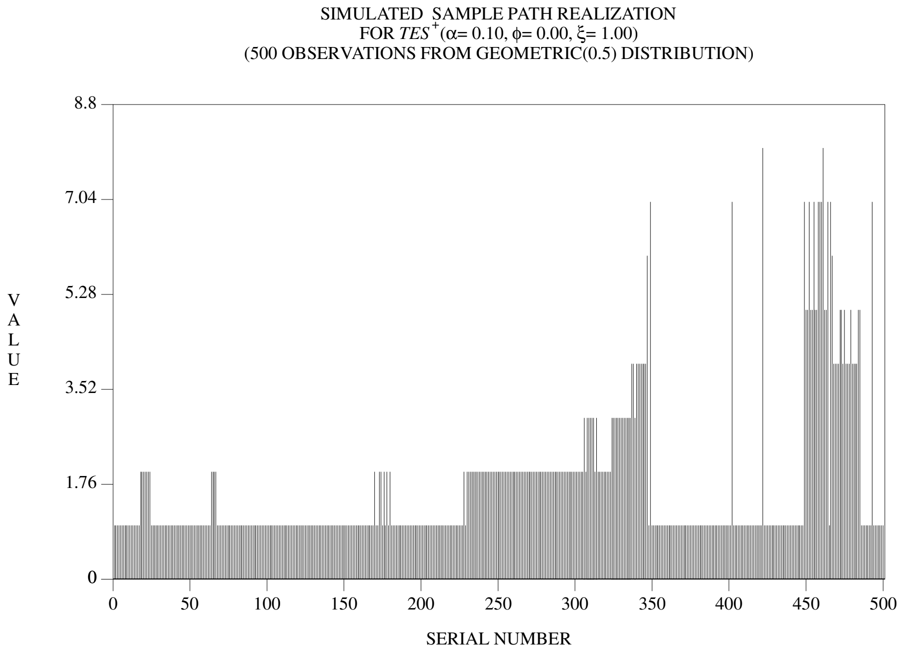

Figure 15: Sample Path of a Geometric TES$^+$ Process Without Drift

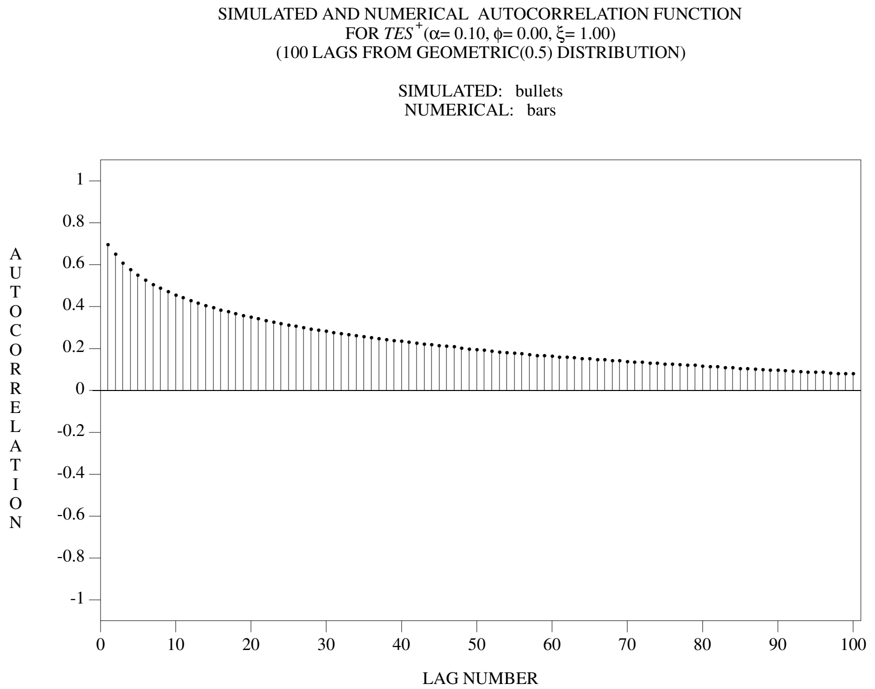

Figure 16: Autocorrelation Functions of a Geometric TES$^+$ Process Without Drift

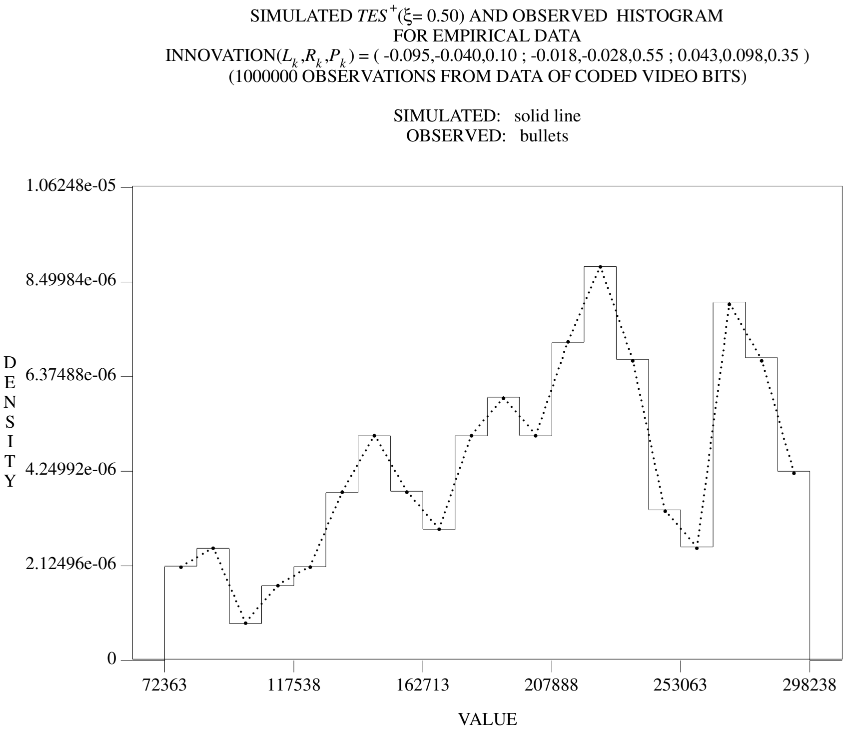

Figure 17: Histograms of Empirical Data and an Empirically Distorted TES Process

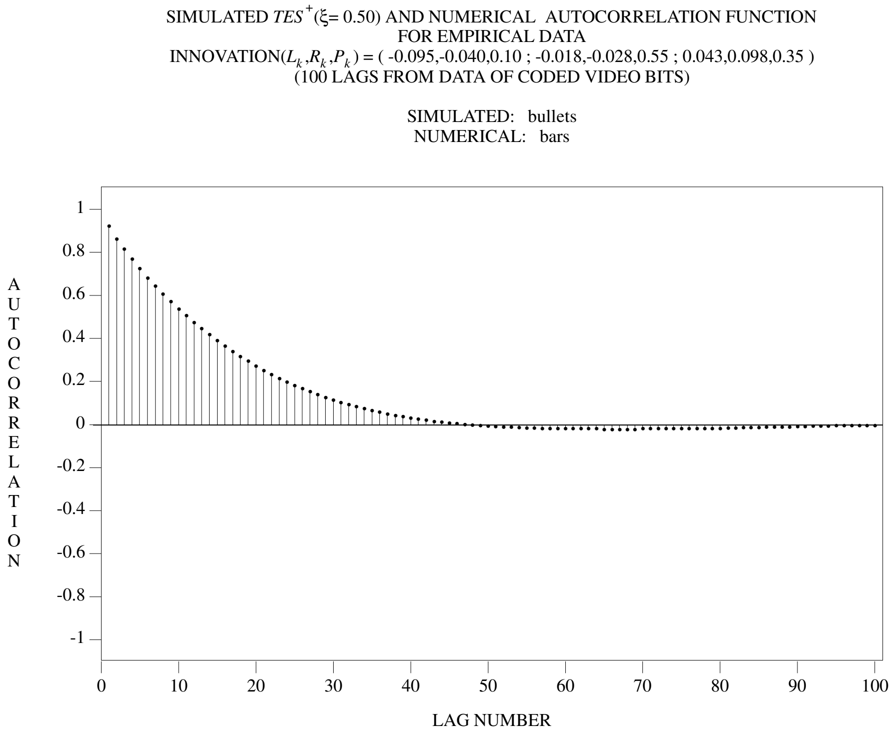

Figure 18: Autocorrelation Functions of an Empirically Distorted TES Process